Journal of Mechatronics, Electrical Power, and Vehicular Technology 16 (2025) 291-304

Journal of Mechatronics, Electrical Power, and Vehicular Technology

e-ISSN: 2088-6985
p-ISSN: 2087-3379

mev.brin.go.id

Low-cost 3D-printed adaptive suspension system for mobile robots using DMP-based real-time stabilization

Sumit Babu Rijal, Prasiddha Chaulagain, Suman Kandel, Tul Bahadur Saru, Srijana Pariyar, Yubraj Bajgain, Kiran Giri *

Department of Mechanical and Automobile Engineering, Pashchimanchal Campus, Institute of Engineering, Tribhuvan University Lamachaur Pokhara 33700, Nepal

Abstract

This paper presents a low-cost adaptive suspension system designed to stabilize a mobile robotic platform operating on uneven terrain. Unlike many existing low-cost servo-based suspension approaches that depend on software-intensive filtering, threshold logic, or extensive tuning, the proposed system adopts a simplified control strategy using hardware-level sensor fusion from the digital motion processor (DMP) of an MPU6050 IMU combined with direct angle-to-actuation mapping. The mechanical design is based on a four-bar linkage suspension architecture actuated by servo motors and controlled using an ESP32 microcontroller, enabling real-time compensation of pitch and roll disturbances. Developed as a proof-of-concept platform with modular 3D-printed components, the system emphasizes accessibility, ease of fabrication, and reduced control complexity. Experimental evaluation under controlled, quasi-static conditions demonstrates effective chassis stabilization with limited angular deviation and consistently lower noise compared to a Kalman filter-based implementation, particularly during post-calibration operation. By balancing mechanical simplicity and additive manufacturing with reliable orientation feedback, the proposed design provides an accessible framework for teaching laboratories, low-budget research, and early-stage adaptive suspension development in resource-constrained environments.

Keywords: adaptive suspension; additive manufacturing; digital motion processor; four-bar linkage; inertial measurement unit; mobile robots.

I. Introduction

Robotics is an extensively recognized discipline today thanks to its demand not exclusively in manufacturing but also across various sectors such as healthcare, forging industries, schools, space exploration, search and rescue missions, and numerous other fields [1]. According to the Robot Institute of America, "A robot is a reprogrammable, multifunctional manipulator designed to move material, parts, tools, or specialized devices, through variable programmed motions for the performance of a variety of tasks" [2]. The continuing evolution of robotics is driven by the growing performance standards posed by sophisticated applications, which range from precision surgical procedures in highly regulated environments to autonomous exploration in extreme and unstructured terrains like Mars [3][4], which typically rely on highly specialized, resource-intensive robotic platforms.

* Corresponding Author. kirang@wrc.edu.np (K. Giri)

https://doi.org/10.55981/j.mev.2025.1315

Received 6 November 2025; revised 9 December 2025; accepted 16 December 2025; available online 30 December 2025; published 31 December 2025

How to Cite: S. B. Rijal *et al.*, "Low-cost 3D-printed adaptive suspension system for mobile robots using DMP-based real-time stabilization," *Journal of Mechatronics, Electrical Power, and Vehicular Technology*, vol. 16, no. 2, pp. 266-279, Dec. 2025.

Robotic systems designed for unstructured and extreme terrains must achieve stability and adaptability to ensure efficient operation. Traditional robotic suspension mechanisms, while effective in conventional mobile robots, often fail to meet the dynamic demands of uneven and unpredictable landscapes. For instance, there is a significant risk of vehicle rollover and immobility on topographies with irregular features that have vertical projections from the ground [5][6]. Therefore, off-road mobility issues can show up in a number of important ways, including decreased stability that could result in rollover, increased wheel slippage that could reduce traction and hinder movement, and the possibility of mechanical damage to the drive systems or chassis of robots and mission compromise [7].

Advanced suspension technologies like the "Rocker-Bogie Mechanism" used in the Mars Curiosity Rover have set benchmarks for terrain adaptability, effectively distributing loads across multiple wheels while maintaining ground contact [8]. However, challenges in achieving seamless terrain navigation persist, particularly when considering the complexity, weight, and cost associated with such systems. Recent research has explored various approaches to active and semi-active suspension systems for mobile robots. These systems were designed to assist robots in moving forward, navigating obstacles, and enhancing their mobility and stability [9]. Adaptive suspension systems provide a solution by dynamically adjusting wheel angles and maintaining optimal ground contact, thereby enhancing mobility, stability, and energy efficiency in robotic and autonomous systems [10]. These systems passively control wheel camber based on suspension travel, enabling vehicles to maintain peak performance across varying terrains [11].

While research on the design and implementation of adaptive suspension systems remains relatively limited, existing studies provide valuable insights that can inform the development of such models. A kinematic control strategy developed by Freitas *et al.* improved stability by 15.5 % and speed by 28 % for an amphibious wheel-legged robot used in environmental monitoring in the Amazon rainforest [12]. A study on four-wheel-legged robot with an integrated suspension system combining active posture control and passive vibration isolation, achieved a 59 % reduction in posture angles and up to 46.7 % reduction in angular acceleration, confirming improved stability and ride comfort [13], but at the cost of increased mechanical and control system complexity. A study done by Jiang *et al.* on a mobile robot resulted in improved stability and smooth operation on unstructured terrains by using an active adjustable suspension system, enabling autonomous self-leveling on slopes up to 12.33° and achieving maximum stability at the lowest ground clearance [14]. Jia *et al.* study on a vehicle attitude control system using four independent series active actuators showed that the system maintained a level body by contracting the front actuators and extending the rear on slopes, and counteracted tilting by extending the left actuator and contracting the right, effectively mitigating pitch and roll through real-time adjustments to enhance stability and payload safety [15]. Wang *et al.* developed an adaptive five-DOF all-terrain robot with gear-driven body joints to modify its posture in real time, thereby demonstrating strong terrain flexibility and the capacity to support loads exceeding 2000 N [16], although such designs require complex mechanical assemblies and high actuation power.

Despite these advances, the most significant challenges in developing mobile robots with adaptive suspension systems remain the complexity of control systems, higher production costs, and extremely complex mechanical assemblies required [3]. These restrictions limit accessibility and hinder innovation, particularly for research institutions, small-scale initiatives, and developing regions where resource constraints should not limit creativity and technological advancement. The excessive costs and complexity of traditional manufacturing methods for custom suspension components create barriers to entry that obstruct widespread adoption of adaptive suspension technology. Recent advances in additive manufacturing (AM) and sensor technology present unprecedented opportunities to address these challenges. Additive manufacturing allows for rapid prototyping, customization, and cost-effective production of complex geometries at considerably lower costs than traditional manufacturing techniques [16][17]. The use of 3D printing enables quick prototyping and continuous testing of different structural designs, facilitating iterative design improvements. In addition to structural fabrication, the choice of state estimation and filtering techniques is equally critical to system performance. Although Kalman filter-based methods are widely used, their various variants differ in terms of simplicity, compatibility, and computational efficiency, which makes their application challenging in highly dynamic or uncertain environments [1]. In contrast, the development of integrated sensor systems, such as digital motion processors (DMPs), offers improved accuracy and reduced computational requirements

compared to traditional filtering approaches like Kalman Filters.

In order to overcome these problems, this study suggests a new, affordable, and clear design that improves robot mobility, stability, and maneuverability without being overly complex or expensive. The research addresses critical technical challenges through the development of a low-cost, 3D-printed adaptive suspension system that uses DMP-based real-time stabilization. The system utilizes a four-bar linkage mechanism actuated by servo motors to dynamically adapt suspension characteristics based on real-time surface feedback from an inertial measurement unit (IMU) MPU6050 and ESP32 microcontroller. The four-bar linkage is selected for its kinematic constraint and ease of additive manufacturing, while the DMP-based IMU is employed to reduce control and tuning complexity through hardware-level sensor fusion. This study works toward making adaptive suspension technology more accessible while maintaining high performance standards. By demonstrating that sophisticated terrain adaptation capabilities can be achieved through the integration of readily available technologies this work opens new possibilities for mobile robotics applications across a wide range of operational environments and resource constraints. The main contributions of this work are summarized as follows:

1. The development of a low-cost, lightweight adaptive suspension architecture that integrates mechanical actuation and sensing within a 3D-printed platform.
2. The formulation of a real-time chassis stabilization approach for compensating pitch and roll disturbances in mobile robotic systems.
3. A systematic comparison of two commonly used orientation estimation strategies for suspension control, highlighting their relative stability and suitability for real-time applications.
4. The experimental demonstration of the proposed concept on a controlled platform, establishing its feasibility as a foundation for future adaptive suspension research.

II. Materials and Methods

A. Electronic components

The adaptive suspension system was built around an ESP32 microcontroller, processing real-time data from the MPU6050 IMU sensor which measures pitch and roll angles to compute necessary corrections and stabilize the chassis. The ESP32 then sends control signals to the servo motors, which dynamically adjust the suspension angles based on pitch and roll feedback, ensuring a balanced platform. Additionally, it regulates the L298N motor driver, controlling the DC motors for robot propulsion, while a buck-boost converter regulates the power supply for consistent performance.

B. Additive manufacturing

Additive manufacturing (AM) process was used for fabrication of components for development of prototype. AM, also commonly known as 3-dimensional (3D) printing, is a manufacturing process that builds objects layer by layer from digital 3D models. Rather than removing materials, AM processes make three dimensional parts directly from CAD models by adding materials layer by layer, as shown in Figure 1, offering the beneficial ability to build parts with geometric and material complexities that could not be produced by current subtractive manufacturing processes [17].

Fused deposition modeling (FDM) is the most commercially available printing technique [18]. It is famous because of its low cost, ease of printing, flexibility in materials, ease of material availability and its applications. The components in this research were fabricated using polylactic acid (PLA) filament, utilizing a Biqu B1 3D printer which is suitable for lightweight prototyping but not intended for high-load applications.

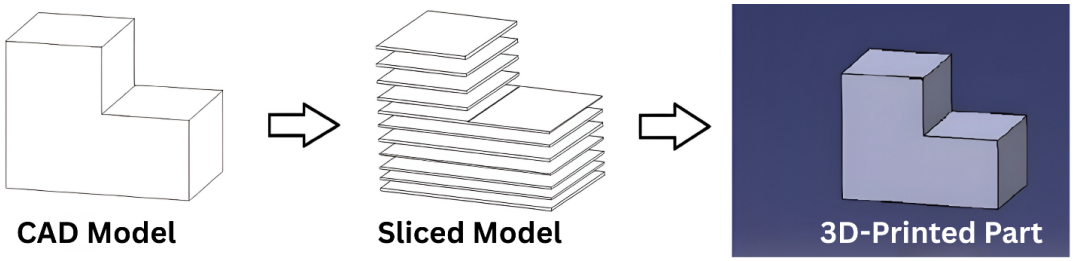

Figure 1. Basic phases of additive manufacturing.

C. System design

1) Mechanical design

The design phase involved creating a detailed CAD model using SolidWorks 2024, with individual components progressively modeled and assembled to ensure proper structure, stability, and mobility in the final 3D design as shown in Figure 2. The mechanical design was constrained to a target payload of approximately 2.7 kg. Although direct load-capacity and long-term fatigue tests were not performed, the design followed conservative engineering margins by limiting the operational load to below 30–40 % of the theoretical maximum torque capacity of the servomotors.

The 3D model of printed circuit board (PCB) was extracted from the KiCad software, which was used to design the circuit. The components have been designed to precisely fit readily available items, such as the servo horn on the driving link, a DC motor on the J-link, and the servo motor on the servo bracket.

Figure 3 shows the individually modeled primary structures of the mobile robot. The J-link is designed to ensure structural integrity by reducing stress concentration while also minimizing the complexity of system.

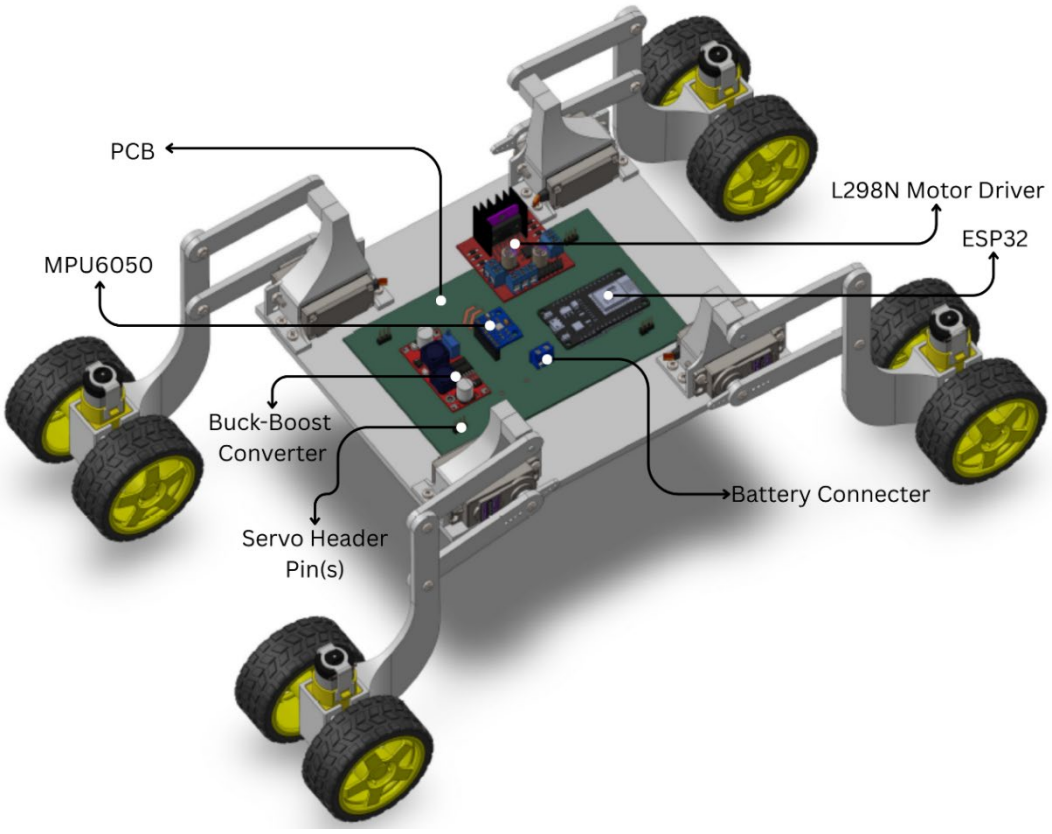

Figure 2. Fully assembled 3D model.

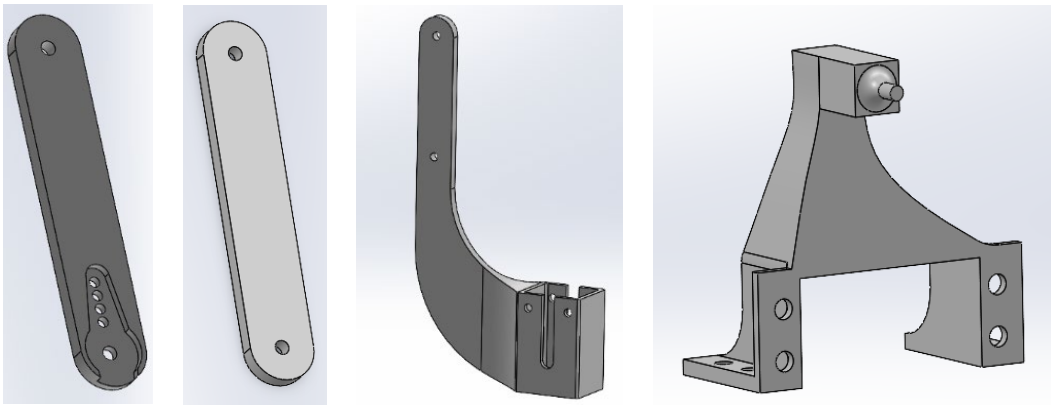

(a) (b) (c) (d)

Figure 3. individually modeled primary structures of the mobile robot. (a) output short link; (b) driving short link; (c) servo bracket; and (d) J-Link.

These parts were integrated to produce a parallel four-bar linkage that controls each leg's adaptive movement. The components have been designed to precisely fit readily available items, such as the servo horn on the driving link, a DC motor on the J-link, and the servo motor on the servo bracket. Figure 4 depicts the assembled quarter-leg, which section serves as the foundation of the entire suspension system, ensuring compactness and mobility while staying easy to manufacture via AM.

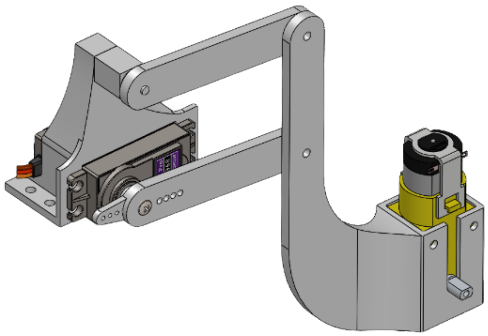

Figure 4. Quarter leg model.

2) Circuit designing

In order to specify the connections between the electronic components and guarantee appropriate power distribution and signal flow, a comprehensive circuit design was created in KiCad software, which is an open-source Electronic Design Automation software. After completing the schematic, KiCad was used to construct the PCB layout as shown in Figure 5. To maximize space utilization, reduce signal interference, and ensure effective power and data line routing, the PCB is carefully laid out. The design transfer onto the copper clad was conducted using the etching process, which involves selectively removing unwanted copper to create the desired circuit patterns.

The ESP32 microcontroller was solely powered with a 5 V power supply from the laptop which provides clean and disturbance free signal. If the power between ESP32 and other electronics is shared, there is a high chance that the servo motor jitters extremely, and the controller might restart erratically due to power inefficiency. This is because, at startup for a noticeably brief time, the servos draw maximum stall current of 2 A which creates shortage and the controller restarts. And to avoid this, all the other electronics except ESP32 was powered with 12 V – 40 C (1500 mAH) Li-Po battery. Since the servos have maximum rated voltage of 6.7 V, buck-boost converter was used to step down the voltage to 6 V. It was recommended to avoid converter and use suitable power source for effective operation of all electronics.

A single L298N motor driver was used to control the four DC motors. Usually, two drivers are used for independent control of four motors, but the control logic was so optimized that one driver was enough to control them. Due to this, the mobile robot did not have

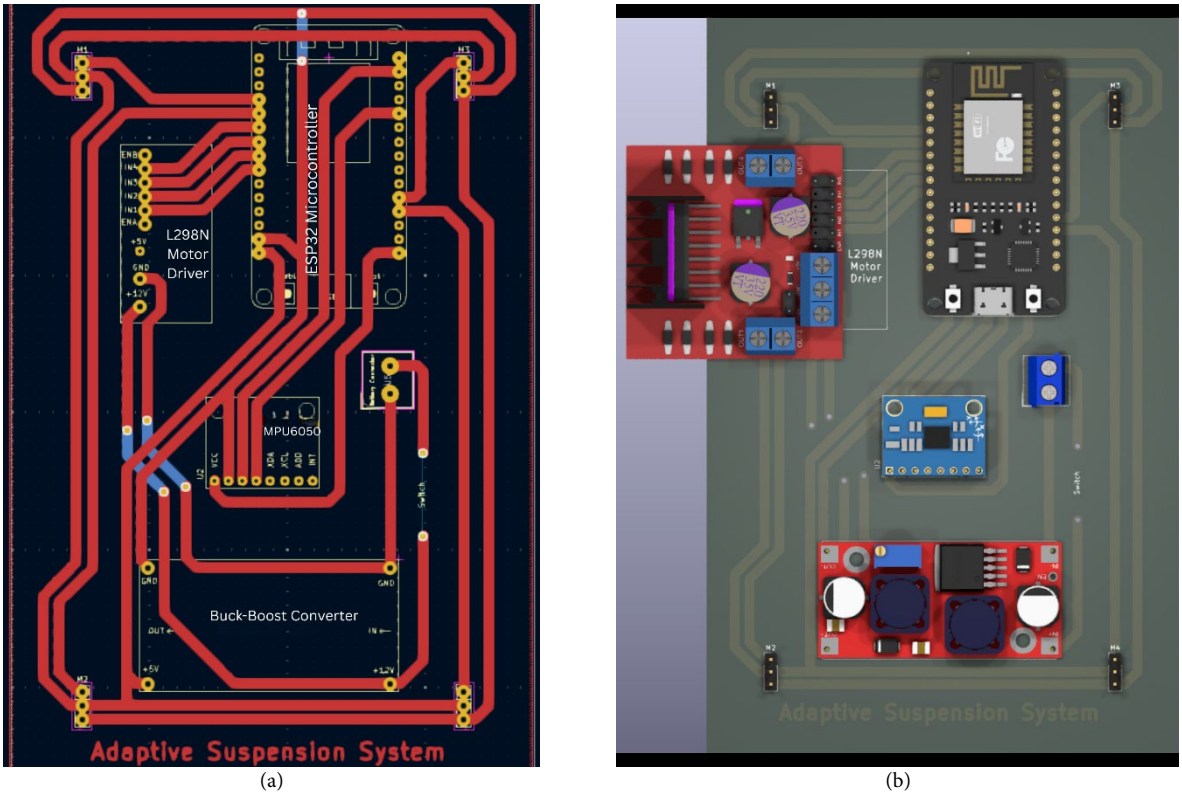

(a) (b)

Figure 5. PCB layout; (a) schematic circuit diagram; and (b) placement of electronics.

steering mechanism. The approach was adopted not only to simplify the system but also to minimize overall power consumption.

D. Control system

The key elements of the control system include the IMU (MPU6050), microcontroller (ESP32), potentiometer feedback from the actuators and the actuators (servos) themselves. The control algorithm loop is shown in Figure 6. The overall aim of the control system is to maintain a horizontal position of the chassis autonomously by recovering from each individual pitch and roll angles and maintain a constant or variable ground clearance depending upon the obstacle [19], with this study focusing specifically on stabilization behavior rather than full obstacle negotiation or ground-clearance optimization.

The MPU6050 sensor has a DMP that executes complex six-axis Motion Fusion algorithms. The inner DMP employs a high-performance process to combine accelerometer as well as gyroscope measurement data and produce an attitude quaternion that exhibits excellent real-time performance [20]. In this work, the DMP output is evaluated directly within an adaptive suspension control loop and compared against a Kalman Filter under identical operating conditions.

Three successive rotations are used to express orientation via Euler angles: roll (around the X-axis), pitch (around the Y-axis), and yaw (around the Z-axis). Despite being simple, this approach may be prone to gimbal lock, a circumstance when two rotating axes line up and one degree of freedom is lost.

A quaternion (q), on the other hand, uses four parameters to represent direction. The axis of rotation is defined by three i.e. $r_x, r_y, and\ r_z$, and the magnitude of rotation about that axis is defined by the fourth i.e. θ as shown in Figure 7. Quaternions are perfect for instances such as sensor fusion in IMUs because of their small, singular rotation, which prevents gimbal lock and permits smooth interpolation [21][22]. A unit quaternion is given by, $q = (q_w, q_x, q_y, q_z)$ where, $q_w = \cos\left(\frac{\theta}{2}\right)$ is the real (scalar) and $\begin{bmatrix} q_x \\ q_y \\ q_z \end{bmatrix} = \begin{bmatrix} \sin\left(\frac{\theta}{2}\right) r_x \hat{\imath} \\ \sin\left(\frac{\theta}{2}\right) r_y \hat{\jmath} \\ \sin\left(\frac{\theta}{2}\right) r_z \hat{k} \end{bmatrix}$ is the imaginary (vector) part.

A quaternion representing rotation by angle θ around a unit vector $\vec{r} = (r_x, r_y, r_z)$ is given by equation (1):

$$q(\theta, \vec{r}) = \cos\left(\frac{\theta}{2}\right) + \sin\left(\frac{\theta}{2}\right)(r_x\hat{\imath} + r_y\hat{\jmath} + r_z\hat{k}) \quad (1)$$

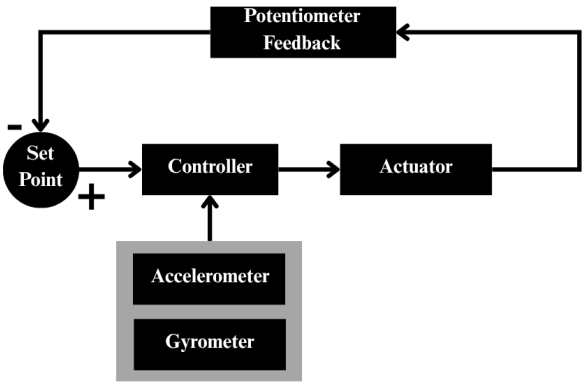

Figure 6. Control loop of adaptive system.

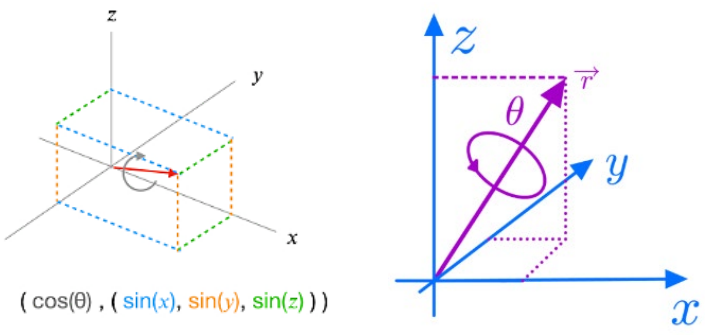

(a) (b)

Figure 7. (a) 3D quaternion orientation; and (b) 2D quaternion orientation.

Once the quaternion orientation parameters are obtained, we calculate the gravity vector using equation (2), (3), and (4) so that we can calculate the required Euler angles using equation (5) and equation (6). Gravity vector is the assumed direction of gravity in the sensor's local coordinate system when the sensor rotates, however gravity vector always directs downward from a global perspective.

Gravity vector is represented by, $\vec{g} = (g_x, g_y, g_z)$, where individual components along the x, y and z-axis are calculated as equation (2) to equation (4):

$$g_x = 2(q_x q_z - q_w q_y) \tag{2}$$

$$g_y = 2(q_w q_x + q_y q_z) \tag{3}$$

$$g_z = (q_w^2 - q_x^2 - q_y^2 + q_z^2) \tag{4}$$

From these x, y, and z gravity vector components, we calculate the required Euler angles using equation (5) to equation (6):

$$Pitch(\phi) = atan\left(\frac{g_x}{\sqrt{(g_y^2+g_z^2)}}\right) \tag{5}$$

$$Roll(\delta) = atan\left(\frac{g_y}{\sqrt{(g_x^2+g_z^2)}}\right) \tag{6}$$

As soon as the ESP32 receives pitch and roll information from the MPU6050, it assesses the angles and operates the actuators accordingly. The orientation is continuously tracked by the closed-loop feedback control system, which uses real-time calculations to account for any deviation from the intended setpoint. Based on that difference, suitable control signals are created to rectify the alignment using servo actuation.

E. Dynamic modeling

To understand how the adaptive suspension behaves under different road conditions, a dynamic model of the system is developed. Without mentioning the general assumptions made to model the active/adaptive suspension, certain key assumptions were made to simplify the modeling of the mobile robot. They are:

- The J-link is modeled as a linear spring-damper unit with exceedingly high stiffness (K_s) and damping coefficient (C_s) for force transmission between spring and unsprung mass.
- The horizontal displacement (x-axis) of the linkage during adaptation is neglected, and only vertical displacement (y-axis) is considered.
- The servo's torque output is modeled as a force component (F_a) acting only vertically on the sprung mass through the link.

The conceptual model of our adaptive suspension system is shown in Figure 8. If Z_r is the road displacement input, Z_u and Z_s represent the unsprung and sprung mass displacement, respectively. In addition, the tire is represented as a mass (m_u) having compressibility or stiffness of K_t.

The equations of motion for the mobile robot's quarter-car model adaptive suspension system can be derived using Newton's laws and are represented as,

For a sprung mass is given by equation (7),

$$m_s\ddot{Z}_s = K_s(Z_u - Z_s) + C_s(\dot{Z}_u - \dot{Z}_s) + F_a \tag{7}$$

For an unsprung mass is given by equation (8),

$$m_u\ddot{Z}_u = -K_s(Z_u - Z_s) - C_s(\dot{Z}_u - \dot{Z}_s) + K_t(Z_r - Z_u) - F_a \tag{8}$$

where, $\ddot{Z}_s$ and $\ddot{Z}_u$ represent acceleration of sprung and unsprung mass and, $\dot{Z}_s$ and $\dot{Z}_u$ represent velocity of sprung and unsprung mass, respectively.

The linear representation of our dynamic suspension system in state-space form can be written as equation (9),

$$\dot{x} = Ax + Bu \tag{9}$$

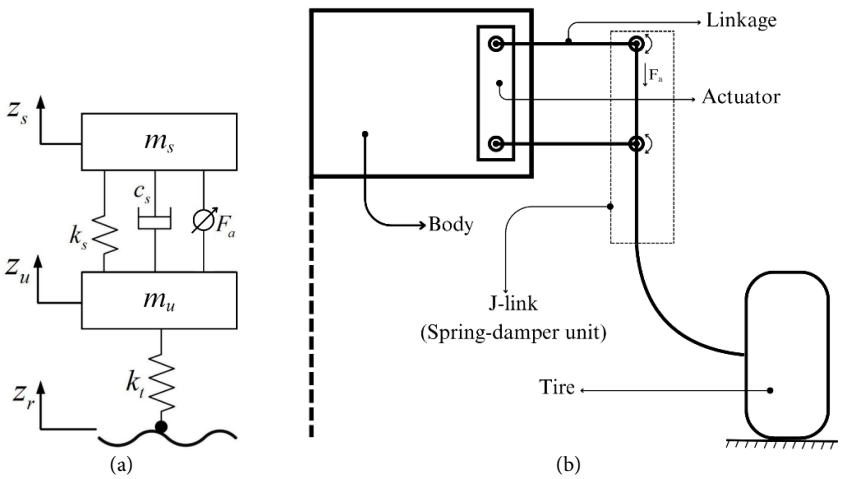

Figure 8. (a) Conceptual model of the adaptive suspension system; and (b) 2D quarter leg design.

Four state variables are defined as:

$$x_1 = Z_s \mid x_2 = \dot{Z}_s \mid x_3 = Z_u \mid x_4 = \dot{Z}_u$$

State variables are set of variables that can describe the system's current condition at any time, given the inputs are known. Especially for mechanical systems, the position and velocity for each mass are chosen. So, the state vector becomes equation (10):

$$x = \begin{bmatrix} Z_s \\ \dot{Z}_s \\ Z_u \\ \dot{Z}_u \end{bmatrix} = \begin{bmatrix} x_1 \\ x_2 \\ x_3 \\ x_4 \end{bmatrix} \tag{10}$$

Similarly, the input vector which includes road surface displacement and velocity key inputs is represented by equation (11),

$$u = \begin{bmatrix} F_a \\ Z_r \end{bmatrix} \tag{11}$$

From definitions, are represented by equation (12) to equation (13),

$$\dot{x_1} = \dot{Z_s} = x_2 \tag{12}$$

$$\dot{x_3} = \dot{Z_u} = x_4 \tag{13}$$

From sprung mass equation (7), can be written as equation (14),

$$\dot{x_2} = \frac{1}{m_s}[K_s(x_3 - x_1) + C_s(x_4 - x_2) + F_a] \tag{14}$$

From unsprung mass equation (8), can be written as equation (15),

$$\dot{x_4} = \frac{1}{m_u}[K_s(x_1 - x_3) + C_s(x_2 - x_4) + K_t(Z_r - x_3) - F_a] \tag{15}$$

Now, matrices A and B can be calculated from the above equation (12) to equation (15),

$$A = \begin{bmatrix} 0 & 1 & 0 & 0 \\ -\frac{K_s}{m_s} & -\frac{C_s}{m_s} & \frac{K_s}{m_s} & \frac{C_s}{m_s} \\ 0 & 0 & 0 & 1 \\ \frac{K_s}{m_u} & \frac{C_s}{m_u} & -\frac{K_s+K_t}{m_u} & -\frac{C_s}{m_u} \end{bmatrix} \text{ and}$$

$$B = \begin{bmatrix} 0 & 0 \\ \frac{1}{m_s} & 0 \\ 0 & 0 \\ -\frac{1}{m_u} & \frac{K_t}{m_u} \end{bmatrix}$$

And finally, the output equation where positions of both masses, Z_s and Z_u are considered output is given by equation (16),

$$y = Cx \tag{16}$$

where, output vector $y = \begin{bmatrix} Z_s \\ Z_u \end{bmatrix} = \begin{bmatrix} x_1 \\ x_3 \end{bmatrix}$ and output matrix $C = \begin{bmatrix} 1 & 0 & 0 & 0 \\ 0 & 0 & 1 & 0 \end{bmatrix}$.

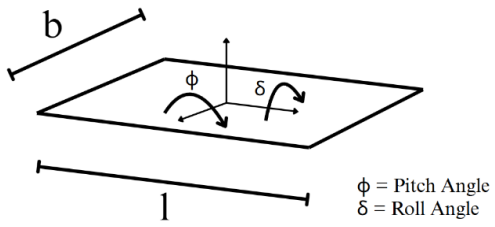

Figure 9. Pictorial representation of angles.

F. Mathematical modeling

The performance of the adaptive suspension system is evaluated based on its ability to compensate for roll and pitch angles, which define the chassis' orientation relative to the terrain. Pitch angle (ϕ) represents the forward or backward tilt of the chassis, while roll angle (δ) refers to its sideways tilt.

Figure 9 illustrates these angles along with the key parameters used in the analysis:

- l = Distance between the front and rear wheel centers
- b = Distance between the left and right wheel centers
- d = Maximum height of a bump that the suspension system can accommodate

Without an adaptive suspension, the maximum pitch and roll angles a chassis can experience are determined by the geometric constraints of the system and are given by equation (17) and equation (18):

$$\phi_{max} = tan^{-1}\left(\frac{d}{l}\right) \tag{17}$$

$$\delta_{max} = tan^{-1}\left(\frac{d}{b}\right) \tag{18}$$

To correct this instability, the pitch and roll values were linearly mapped using linear interpolation, to corresponding range of microsecond values. Since the servo rotation range is from +45 to -45 degrees, it should be mapped in relation to its microsecond value as equation (19) and equation (20) [23],

$$Pitch\ Correction, (\Delta\phi) = \frac{(\phi+\phi_{max})\cdot\mu_{secmax}}{\phi_{max}} - \mu_{secmax} \tag{19}$$

$$Roll\ Correction, (\Delta\delta) = \frac{(\delta+\delta_{max})\cdot\mu_{secmax}}{\delta_{max}} - \mu_{secmax} \tag{20}$$

where, μ_{secmax} = Maximum microsecond value taken for corrections

Independent corrections are required as pitch and roll corrections are independent as they are at right angles. Since servo motors rotation differs from each other due to their placement, Table 1 elaborates their actuations for pitch and roll correction.

Front two and left back servos were used, and right rear servo was set and operated on neutral condition. The process flowchart for receiving pitch/roll data and actuating servos is shown in Figure 10.

Table 1.
Tabulated actuation for different conditions.

Actuation	Pitch	Roll
LF Wheel	$\theta_{current} = \theta_{current} + \Delta\phi$	$\theta_{current} = \theta_{current} + \Delta\delta$
RF Wheel	$\theta_{current} = \theta_{current} - \Delta\phi$	$\theta_{current} = \theta_{current}$
LB Wheel	$\theta_{current} = \theta_{current}$	$\theta_{current} = \theta_{current} - \Delta\delta$

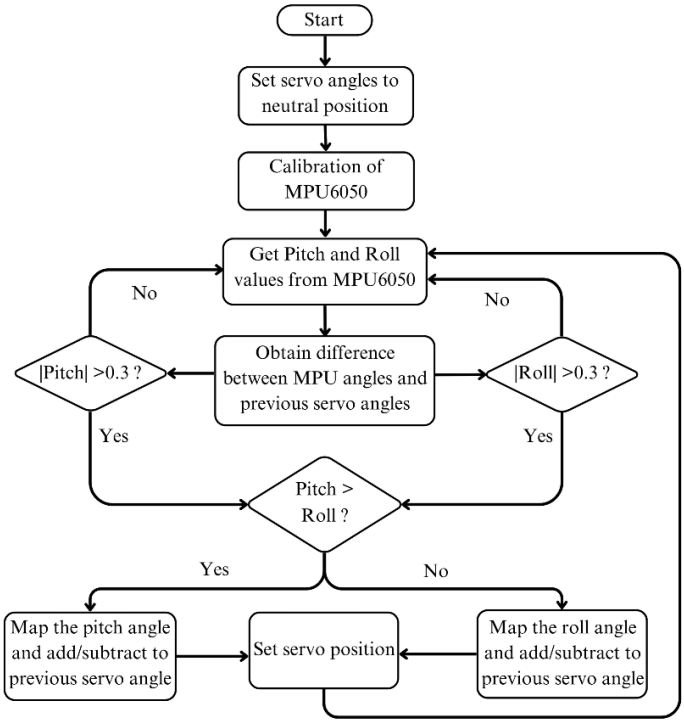

Figure 10. Flowchart for sensor data flow and servo.

III. Results and Discussion

A. Comparative analysis of DMP and Kalman Filter

The comparative analysis between the DMP and the Kalman Filter for pitch and roll measurements reveals significant differences in stability and fluctuation behavior. The DMP data maintains steady fluctuations within a narrow range of ±0.03°, ensuring consistent and reliable readings. In contrast, the Kalman Filter exhibits higher fluctuation levels, reaching ±0.08°, which indicates increased instability. Although the numerical difference between the observed fluctuations appears small, its impact on suspension control is significant. In a closed-loop stabilization system, higher fluctuation levels lead to frequent micro-corrections at the actuator level, resulting in unnecessary servo activity and reduced holding stability. More importantly, the fluctuations in the Kalman Filter are not steady, displaying irregular variations over time and also, after calibrating the sensor, the initial readings showed a clear difference in stability, with the DMP data fluctuating within ±0.01°, compared to Kalman Filter's ±0.1°, a tenfold improvement right from the beginning.

The plotted Kalman filter output shown in Figure 11 shows erratic spikes and unpredictable deviations, while the DMP data shown in Figure 12 follows a controlled variation pattern. The provided graph and fluctuation data visually confirm the superior stability of the DMP, as its readings remain smoother and more controlled. This difference in fluctuation behavior highlights the impact of each filtering method on system performance, with DMP demonstrating clear advantages in ensuring consistent sensor data for chassis stabilization.

The study on controlling gimbal stability by Crisnapati *et al.* [24] also demonstrated the superiority of DMP over Kalman Filter, with DMP achieving an accuracy rate of 99.3 % and an average error of 0.7096. This outperforms Kalman Filter, which achieved an accuracy rate of 67.55 % with an error of 33.35 [24]. The major factor that contributes to the superiority of DMP is its quaternion-based sensor fusion internally. The process of measuring pitch and roll with Kalman Filter

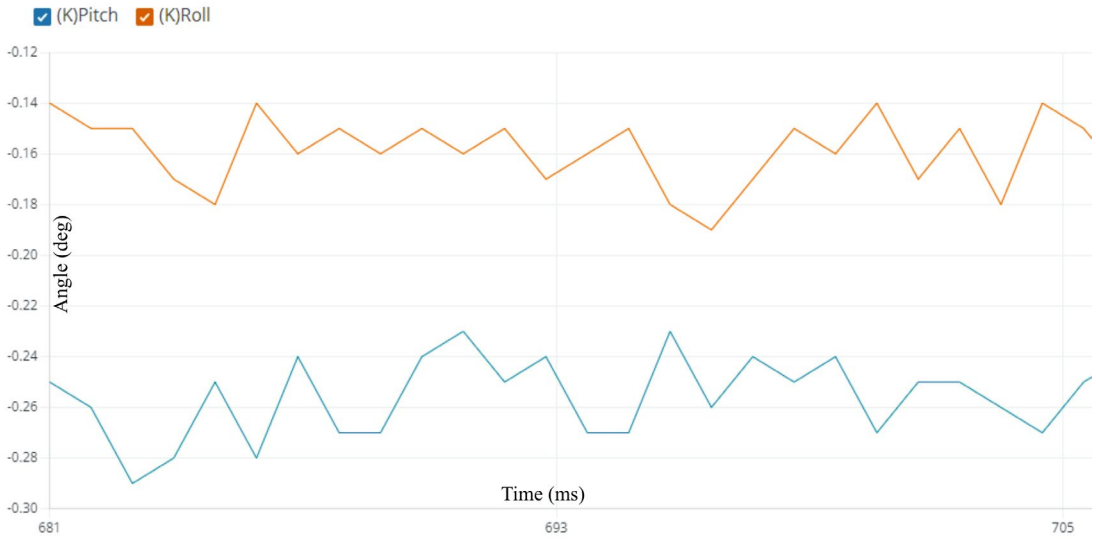

Figure 11. MPU6050 noise with Kalman Filter.

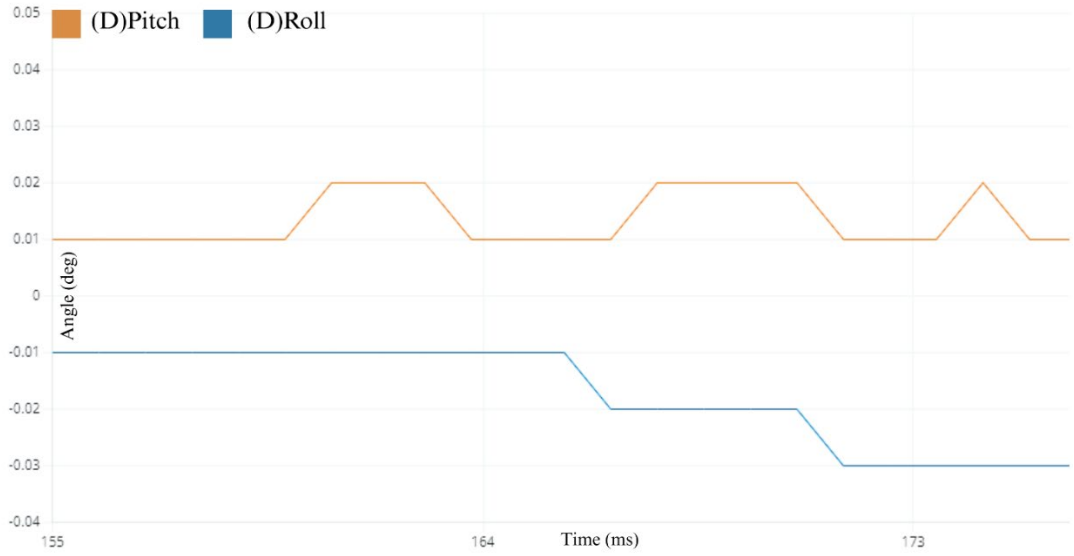

Figure 12. MPU6050 noise with DMP.

implementation is quite straightforward as it directly uses the raw accelerometer and gyroscope data, while DMP uses gravity vector which greatly reduces the computational time and complexity.

Kalman is a recursive filter which repeats two steps at every time step "t". The time update projects the current state estimate ahead in time and the measurement update adjusts the projected estimate by an actual measurement at that time [25]. The uncertainty grows during the prediction step due to noise but again decreases when a measurement update was acquired, and this process operates in loop (Figure 13) to bring the system to a more accurate orientation with each loop. Better results can also be obtained using Kalman Filter by fine tuning the adjustable parameters; Process noise covariance (Q) and Measurement noise covariance (R), but this

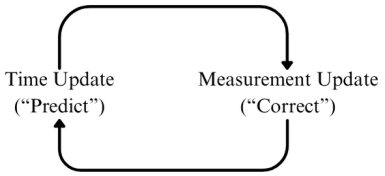

Figure 13. Kalman Filter loop [26].

increases the load on CPU and can also decrease the update frequency [26].

The fluctuations in Kalman Filter graph as seen in Figure 11 is due to multiple limitations like poor Kalman Gain tuning and inconsistent timing between measurement. While setting more weight to the accelerometer leads to a more accurate but noisy measurement and giving the gyroscope more weight yields a smoother but slower signal [27].

B. Findings of the study

When the model climbs over an obstacle and experiences pitch change, as shown in Figure 14, the system balances the change iteratively with the change margin reaching a maximum of 1.5°. The roll also experiences change, but it is neglected due to extremely small variation. Similar is the case for roll correction in Figure 15, where small variations in pitch value are neglected. As evident from the graph and also considering some degree of inaccuracy in servo movements, the overall accuracy of the system is about 1.5°. The observed stabilization response indicates that residual vibrations do not propagate into sustained actuator motion, allowing the chassis to remain level after correction. Since 1.5° seems exceedingly small value, it is the relative tilt value of the IMU sensor with respect to the tilt of whole platform of the robot which obviously experiences greater tilt than 1.5°.

As it is possible to observe in Figure 16, there is adjustment of pitch value in dark green (adjusted line) and the roll value in soft green (straight line). From analyzing the graph, it can be concluded that from point A to point B there are twelve of the units on the

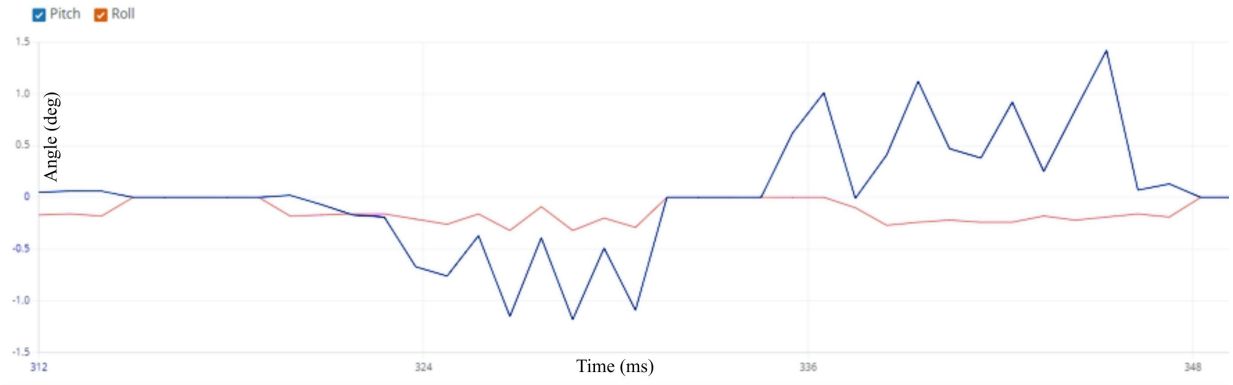

Figure 14. Pitch correction (blue).

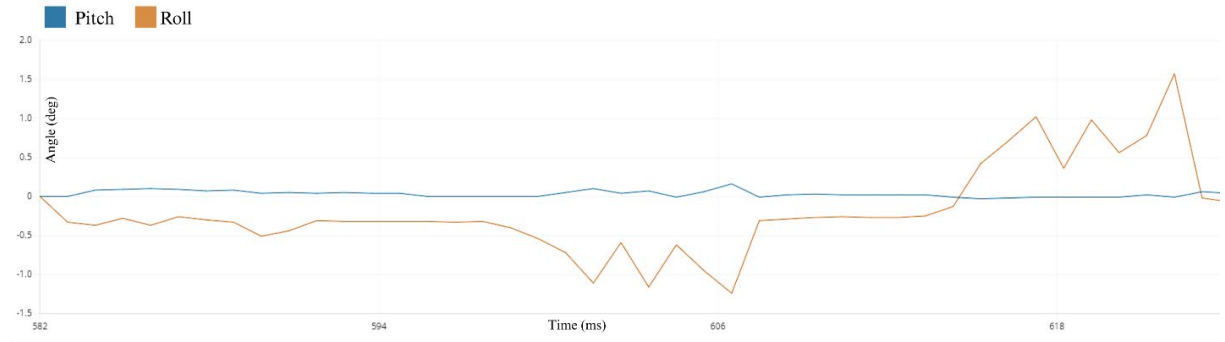

Figure 15. Roll correction (yellow).

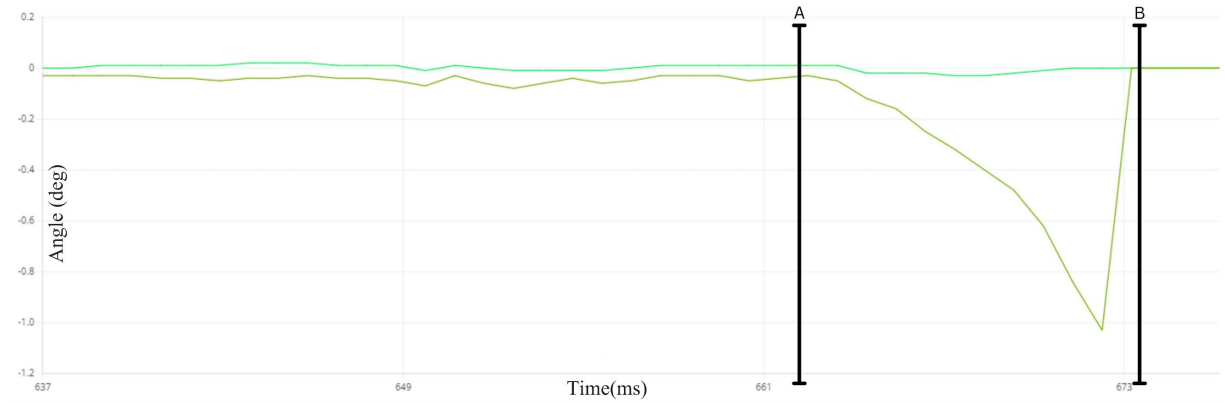

Figure 16. Response time.

x-axis which represent each loop with recorded data. Can be written as equation (21),

$$T_{stabilizing} = gap * T_{delay} \quad (21)$$

where T_{delay} = Time delay in ms kept in the code before it takes new reading, $T_{stabilizing}$ = Time in ms required to bring the adjustment value within deadband, and $T_{stabilizing} = 240\ ms$.

To understand the system's reaction, the results were put against a study done by Dubrovsky [28]. In this work, the stabilized attitude with servo actuated platforms and the measured stabilization times were 1106 ms and 2048 ms for pitch and roll, respectively. His system used a different control plan, it forced pitch and roll values to zero when they stayed within a ±3° range, compared to ±0.3° in our work. This method prefers steady state suppression, but it causes delay which comes from deadband handling based on a threshold and from slower convergence.

The observed stabilizing time of 240 ms reflects the combined efficiency of the DMP-centered orientation estimation and the relatively simple interpolation-based control algorithm. It should be noted that this response time does not account for potential overshoot, as the DC motors used for propulsion lacked sufficient torque to drive the robot at meaningful speeds. This limitation can be observed in the roll and pitch adjustment graphs, where the lack of significant movement affects the dynamic response. Nevertheless, the robot successfully demonstrated the intended functionality of the adaptive suspension system and provided valuable insight into its behavior under control.

The proposed adaptive suspension system was evaluated in terms of pitch and roll stabilization under quasi-static conditions. Dynamic movement was not evaluated; only theoretical aspects of response to dynamic inputs are discussed. Based on experimental data from several trials:

- **RMS error:** The system maintained a root-mean-square (RMS) error of ±0.03° in both pitch and roll using DMP-based stabilization, while a standard Kalman filter showed ±0.08° fluctuations.
- **Maximum overshoot & settling time:** Since dynamic motion was not tested physically, these metrics are discussed theoretically. Based on model-scale simulations, the overshoot is expected to be minimal due to the fast response of servo motors, and settling time is estimated to be within 0.2–0.3 s for small-angle disturbances.
- **Noise and stability:** The DMP-based system exhibits steady fluctuations, demonstrating low noise and stable performance.

C. Comparison with closely related studies

Compared with closely related adaptive and stabilized suspension systems reported in the literature, the proposed system emphasizes a balanced trade-off between mechanical complexity, control performance, and accessibility. The stabilized driving platform [28] uses a simplified framework with only two servomotors for pitch and roll control, accomplishing stabilization errors of about ±2.9° and response times ranging from 1.1 s (pitch) to 2.0 s (roll). This makes it well suited to learning and preliminary demonstrations of active stabilization principles rather than complete chassis-level suspension control. In contrast, rover-scale systems such as the Rudra Mars Rover [19] use four high-stroke linear actuators and emphasized axis resolution approaches to handle large payloads and extreme terrain, but do not explicitly report stabilization response or fine angular accuracy, indicating a preference for robustness over rapid closed-loop correction. Similarly, the adaptable all-terrain robot [16] exhibits great load-bearing capabilities and multi-DOF posture modification via gear-driven joints, at the expense of additional mechanical and control complexity. This study shows that a lightweight, servo-actuated four-bar linkage developed with low-cost FDM 3D printing can achieve sub-degree stabilization accuracy (within ±1.5°) and fast static response (≈240 ms), making it a practical proof-of-concept for rapid, resource-constrained robotic platforms rather than mission-ready rover systems.

This simplicity, low cost, and use of readily available components make our approach highly accessible for teaching labs, low-budget research projects, and applications in developing countries where resources are limited, providing a practical platform for hands-on learning of adaptive suspension systems.

IV. Conclusion

The proposed adaptive suspension system effectively stabilizes the chassis, maintaining balance during obstacle traversal and limiting pitch and roll deviations. The DMP-based sensor consistently provides reliable and steady feedback, outperforming the standard Kalman Filter, and enabling precise tilt compensation. Fabrication using 3D-printed modular components reduces material usage and assembly time, demonstrating the practicality of the design. The system's rapid response is facilitated by hardware-level sensor fusion and direct angle-to-PWM control, highlighting the efficiency of the implemented control strategy. However, several limitations remain. Dynamic

testing at higher speeds and under significant load has not been conducted, and the full dynamic model has not yet been validated against experimental data. Additionally, PLA-based structures limit long-term mechanical reliability and load-bearing capability, and the current actuators constrain maximum response speed and torque. Future work can address these limitations by integrating high-quality servos or stepper motors for improved actuation, employing engineering-grade materials such as polyethylene terephthalate glycol (PETG), acrylonitrile butadiene styrene (ABS), or aluminum for structural components, and incorporating ball bearings in linkage joints for smoother and more stable motion. Further experiments should validate the dynamic model under realistic operating conditions, including higher speeds, varying loads, and extended operation. Improvements in electrical design, such as independent power sources for microcontrollers and other components, can further enhance system stability. Collectively, these enhancements will make the system more robust, reliable, and suitable for practical applications or teaching laboratories.

Declarations

Author Contribution

S.B. Rijal: Manuscript preparation. **S.B. Rijal, P. Chaulagain, S. Kandel, T.B. Saru, S. Pariyar & Y. Bajgain**: Mathematical modeling, mechanical design, circuit design, fabrication, experimentation, and data collection. **K. Giri**: Supervision, manuscript review and editing the manuscript. All authors reviewed and approved the definitive version of the manuscript.

Funding statement

This research did not receive any specific grant from funding agencies in the public, commercial, or not-for-profit sectors.

Competing interest

The authors declare that they have no known competing financial interests or personal relationships that could have appeared to influence the work reported in this paper.

The use of AI or AI-assisted technologies

The authors declare that no AI or AI-assisted technologies were used.

Additional information

Reprints and permission: information is available at https://mev.brin.go.id/.

References

[1] M. H. Gusrial, N. A. Othman, H. Ahmad, and M. H. A. Hassan, "Review of Kalman Filter variants for SLAM in mobile robotics with linearization and covariance initialization," *J. Mechatron. Electr. Power Veh. Technol.*, vol. 16, no. 1, pp. 69–83, Jul. 2025.

[2] D. M. Considine and G. D. Considine, "Robot technology fundamentals," in *Standard Handbook of Industrial Automation*, D. M. Considine and G. D. Considine, Eds., Boston, MA: Springer US, 1986, pp. 262–320.

[3] R. Gamage, C. Rathnayake, R. Kalubowila, and S. Thilakarathne, "Design and development of a quarter-car model active suspension system for a mobile robot to enhance terrain adaptability with better stability and mobility," *J. Mechatron. Robot.*, vol. 8, no. 1, pp. 39–48, Jan. 2024.

[4] M. Nikolova, F. Cnossen, and B. Nikolaev, "Robots, meaning, and self-determination," *Res. Policy*, vol. 53, no. 5, p. 104987, Jun. 2024.

[5] P. V. K. Borges *et al.*, "A Survey on terrain traversability analysis for autonomous ground vehicles: methods, sensors, and challenges," *Field Robot.*, vol. 2, pp. 1567–1627, Jul. 2022.

[6] H. Lee, T. Kim, J. Mun, and W. Lee, "Learning terrain-aware kinodynamic model for autonomous off-road rally driving with model predictive path integral control," 2023.

[7] A. Datar, C. Pan, M. Nazeri, and X. Xiao, "Toward wheeled mobility on vertically challenging terrain: platforms, datasets, and algorithms," in *2024 IEEE International Conference on Robotics and Automation (ICRA)*, Yokohama, Japan: IEEE, May 2024, pp. 16322–16329.

[8] C. Cosenza, V. Niola, S. Pagano, and S. Savino, "Theoretical study on a modified rocker-bogie suspension for robotic rovers," *Robotica*, vol. 41, no. 10, pp. 2915–2940, Oct. 2023.

[9] A. Sujiwa and Suhadata, "Design and construction of a self balancing robot using long range control based on NRF24L01," *BEST J. Appl. Electr. Sci. Technol.*, vol. 5, no. 2, pp. 34–37, Sep. 2023.

[10] W. Prastiyo and W. Fiebig, "Multibody simulation and statistical comparison of the linear and progressive rate double wishbone suspension dynamical behavior," *Simul. Model. Pract. Theory*, vol. 108, p. 102273, Apr. 2021.

[11] G. Reina and M. Foglia, "An adaptive suspension system for planetary rovers," *IFAC Proc. Vol.*, vol. 43, no. 16, pp. 199–204, 2010.

[12] G. Freitas, F. Lizarralde, L. Hsu, and N. R. S. D. Reis, "Kinematic reconfigurability of mobile robots on irregular terrains," in *2009 IEEE International*

Conference on Robotics and Automation, Kobe: IEEE, May 2009, pp. 1340–1345.

[13] L. Ni, F. Ma, and L. Wu, "Posture control of a four-wheel-legged robot with a suspension system," *IEEE Access*, vol. 8, pp. 152790–152804, 2020.

[14] H. Jiang, G. Xu, W. Zeng, F. Gao, and K. Chong, "Lateral stability of a mobile robot utilizing an active adjustable suspension," *Appl. Sci.*, vol. 9, no. 20, p. 4410, Oct. 2019.

[15] W. Jia, W. Zhang, F. Ma, and L. Wu, "Attitude control of vehicle based on series active suspensions," *Actuators*, vol. 12, no. 2, p. 67, Feb. 2023.

[16] Z. Wang, J. Zhao, and G. Zeng, "Modeling, simulation and implementation of all terrain adaptive five DOF robot," *Sensors*, vol. 22, no. 18, p. 6991, Sep. 2022.

[17] L. Ben Said, B. Ayadi, S. Alharbi, and F. Dammak, "Recent advances in additive manufacturing: a review of current developments and future directions," *Machines*, vol. 13, no. 9, p. 813, Sep. 2025.

[18] M. V. D. Sai Kalyan, H. Kumar, and L. Nagdeve, "Latest trends in additive manufacturing," *IOP Conf. Ser. Mater. Sci. Eng.*, vol. 1104, no. 1, p. 012020, Mar. 2021.

[19] K. Vaish, S. M. Rajesh, K. Pasupatheeswaran, M. K. Sharma, and V. B. Semwal, "Design and autonomous control of the active adaptive suspension system of Rudra – Mars Rover," *Int. J. Hybrid Inf. Technol.*, vol. 7, no. 3, pp. 249–264, May 2014.

[20] M. Kamal Mazhar, M. J. Khan, A. I. Bhatti, and N. Naseer, "A novel roll and pitch estimation approach for a ground vehicle stability improvement using a low cost IMU," *Sensors*, vol. 20, no. 2, p. 340, Jan. 2020.

[21] Programming Robots, "The MPU6050 explained," Programming Robots. Accessed: Jun. 09, 2025. [Online].

[22] X. Chen, Z. Xie, Y. Eun, A. Bettens, and X. Wu, "An observation model from linear interpolation for quaternion-based attitude estimation," *IEEE Trans. Instrum. Meas.*, vol. 72, pp. 1–12, 2023.

[23] Arduino, "map() | Arduino documentation." Accessed: May 23, 2025. [Online].

[24] P. N. Crisnapati, D. Maneetham, Y. Thwe, and M. M. Aung, "Enhancing gimbal stabilization using DMP and Kalman Filter: A low-cost approach with MPU6050 sensor," in *2023 11th International Conference on Cyber and IT Service Management (CITSM)*, Makassar, Indonesia: IEEE, Nov. 2023, pp. 1–5.

[25] G. Welch and G. Bishop, "An Introduction to the Kalman Filter," 2006.

[26] C. Yukun, S. Xicai, and L. Zhigang, "Research on Kalman-Filter based multisensor data fusion," *J. Syst. Eng. Electron.*, vol. 18, no. 3, pp. 497–502, Sep. 2007.

[27] Lauszus, "TKJ Electronics » A practical approach to Kalman Filter and how to implement it." Accessed: Jun. 13, 2025. [Online].

[28] D.M. Dubrovsky, "Stabilized driving platform," Czech Technical University, 2023.